





**High-order phonon anharmonicity and thermal conductivity in GaN**Bin Wei <sup>1,2,3,\*</sup> Yongheng Li <sup>2,\*</sup> Wang Li,<sup>1</sup> Kai Wang,<sup>1</sup> Qiyang Sun,<sup>4</sup> Xiaolong Yang <sup>5</sup> Douglas L. Abernathy,<sup>6</sup> Qilong Gao,<sup>7</sup> Chen Li <sup>4,†</sup> Jiawang Hong,<sup>2,‡</sup> and Yuan-Hua Lin<sup>3,§</sup><sup>1</sup>*Henan Key Laboratory of Materials on Deep-Earth Engineering, School of Materials Science and Engineering, Henan Polytechnic University, Jiaozuo 454000, China*<sup>2</sup>*School of Aerospace Engineering, Beijing Institute of Technology, Beijing 100081, China*<sup>3</sup>*State Key Laboratory of New Ceramics and Fine Processing School of Materials Science and Engineering, Tsinghua University, Beijing 100084, People's Republic of China*<sup>4</sup>*Department of Mechanical Engineering, University of California Riverside, Riverside, California 92521, USA*<sup>5</sup>*College of Physics, and Center of Quantum Materials and Devices, Chongqing University, Chongqing 401331, China*<sup>6</sup>*Neutron Scattering Division, Oak Ridge National Laboratory, Oak Ridge, Tennessee 37831, USA*<sup>7</sup>*International Laboratory for Quantum Functional Materials of Henan, School of Physics and Microelectronics, Zhengzhou University, Zhengzhou 450001, China*

(Received 25 February 2024; accepted 8 April 2024; published 25 April 2024)

A comprehensive understanding of phonon transport is essential to develop effective solutions for heat dissipation. Gallium nitride (GaN), a representative of third-generation power semiconductors, has been extensively studied regarding its thermodynamics and lattice dynamics. However, the temperature-dependent phonon properties, especially the anharmonicity at high temperatures, are poorly understood. Here, by combining inelastic neutron scattering (INS) experiments and calculations including the temperature effect based on machine learning potentials, we report the high-order phonon anharmonicity in GaN over a wide temperature range. Our calculations agree well with the experimental phonon dispersion, density of states and entropy, underlining the significance of anharmonicity of GaN at elevated temperatures. Moreover, considering the four-phonon processes, the calculated thermal conductivity is suppressed by 20%, and the anisotropy is also reduced gradually with increasing temperature. Such behavior arises mainly from the large four-phonon scattering channels between 20 and 30 meV, where the critical scattering rule for the three-phonon process is largely restricted at high temperatures. Our study highlights the importance of high-order phonon anharmonicity for thermal transport in GaN and provides a theoretical reference for thermal management in other related semiconductors.

DOI: [10.1103/PhysRevB.109.155204](https://doi.org/10.1103/PhysRevB.109.155204)**I. INTRODUCTION**

Gallium nitride (GaN) is one of the most important third-generation power semiconductors, with excellent power density, high thermal conductivity at room temperature, and other attractive properties [1–3]. Due to the increase in power density, operating frequency, and overall complexity of GaN-based power electronics, the rapid increase in heat flux density limits the development of electronic devices [4–7]. The self-heating effect in AlGaIn/GaN heterostructure [8–11] and the uncontrollable thermal stress fields at high temperatures in GaN have been found, guiding the maximization of the functionality of GaN under such limited circumstances [12]. Therefore, a comprehensive understanding of its thermal characteristics is vital for the design of heat dissipation solutions [13]. This demand has greatly motivated research on the heat transfer of semiconductors, where the phonon property is

an inevitable topic. For GaN, due to the artificial synthesis technique induced defects and dislocations in the single crystal, lattice dynamics experiments could not acquire the pure phonon-phonon information [14,15]. In addition, thermal conductivity measurement techniques, such as time-domain thermoreflectance (TDTR), due to the insensitivity to heat transfer along the in-plane direction, make it difficult to investigate the thermal conduction anisotropy [14–16]. Therefore, a thorough understanding of the anisotropic phonon property is of great benefit for regulating the thermal conductivity of GaN.

Thermodynamics studies of GaN have attracted increasing attention and have been extensively investigated over the past decades [14–19]. Among them, simulations and thermal conductivity measurements were in the majority, while the experimental lattice dynamics were poorly involved, especially its temperature dependence [19,20]. Our previous work reported a matryoshka phonon twinning behavior of GaN using inelastic neutron (INS) and inelastic x-ray scattering, revealing the origin of thermal conductivity anisotropy at room temperature [19]. Considering that GaN usually operates at high temperatures due to its properties, such as high power density [17,18], a deep understanding of phonon

\*These authors contributed equally to this work.

†chenli@ucr.edu

‡hongjw@bit.edu.cn

§linyuh@mail.tsinghua.edu.cn

anharmonicity at high temperatures becomes essential in this system. At high temperatures, the anharmonic effect, especially the fourth-order term, is usually non-negligible and has been reported in many systems, such as BAs [21,22], AgCrSe<sub>2</sub> [23], Li<sub>2</sub>NaBi [24], and Na<sub>2</sub>TlSb [25]. Previous theoretical research deemed the four-phonon interaction important in GaN at high temperatures [14,16]. However, due to the absence of experimental lattice dynamics evidence and the neglect of temperature-induced anharmonicity and thermal expansion in the calculations, the fundamental phonon properties and thermal transport of GaN at high temperatures remain unclear. Thus, state-of-the-art techniques, including simulation and experiment, are urgently needed.

Here, we report the high-order phonon anharmonicity and thermal conductivity of wurtzite structure GaN by the combination of temperature-dependent INS experiments and machine-learning interaction potential (MLIP) based calculation. The optical phonon modes of GaN soften with increasing temperature, accompanied by the large mode Grüneisen parameter. Considering the temperature-induced anharmonicity, the calculated vibrational entropy shows a better agreement with experimental results at high temperatures than that under the harmonic approximation or quasiharmonic approximation framework. This observation underlines the significance of large phonon anharmonicity at elevated temperatures. The increased anharmonicity at higher temperatures also results in more pronounced four-phonon scattering processes. The predicted thermal conductivity of GaN, including the four-phonon scattering process at high temperatures, is closer to the experimental values reported in the literature, where  $\kappa_{zz}$  (out of plane) is still larger than  $\kappa_{xx}$  (in plane). Particularly, the four-phonon scattering channels are significantly enhanced between 20 and 30 meV since the three-phonon channels are largely limited by the critical selection rules, leading to the obvious effect of four-phonon scattering processes on thermal conductivity. Our work deepens the understanding of the temperature dependence of phonon property in GaN.

## II. EXPERIMENT AND CALCULATION

### A. Inelastic neutron scattering measurement

Inelastic neutron scattering measurements of a single GaN sample at 50, 300, and 600 K were conducted using the wide angular-range chopper spectrometer (ARCS) at the Spallation Neutron Source (SNS) at Oak Ridge National Laboratory. The incident neutron energy is 150 meV. Detailed setup parameters for the dispersion measurement can be found in our previous work [19]. A reciprocal space map of elastic scattering ( $-1.5 \leq E \leq 1.5$  meV) measurements shows the excellent quality of our single crystal (Fig. S1 of the Supplemental Material [26]). Phonon density of states (DOS) measurements were performed at 50, 150, 350, 540, and 640 K. The incident neutron energies,  $E_i = 50$  and 150 meV, were used at each temperature to measure the low- and high-energy phonons, respectively. The empty can was measured in identical conditions at all temperatures and used for background subtraction. INS data shown in the present work are normalized by the incoherent scattering of vanadium and corrected for the sample temperature to obtain the imaginary dynamical susceptibility,

$\chi''(\mathbf{Q}, E) = S(\mathbf{Q}, E)/[n_T(E) + 1]$ , where  $n_T(E)$  stands for the Bose distribution, and  $S(\mathbf{Q}, E)$  is the scattering dynamical structure factor [19]:

$$S(\mathbf{Q}, E) \propto \sum_s \sum_\tau \frac{1}{\omega_s} \left| \sum_d \frac{\bar{b}_d}{\sqrt{M_d}} \exp(-W_d) \exp(i\mathbf{Q} \cdot \mathbf{r}_d) \right. \\ \left. \times (\mathbf{Q} \cdot \mathbf{e}_{ds}) \right|^2 \langle n_s + 1 \rangle \delta(\omega - \omega_s) \delta(\mathbf{Q} - \mathbf{q} - \tau) \quad (1)$$

where  $\bar{b}_d$  is neutron scattering length,  $\mathbf{Q} = k - k'$  is the wave vector transfer,  $k'$  and  $k$  are the final and incident wave vector of the scattered particle,  $\mathbf{q}$  is the phonon wave vector,  $\omega_s$  is the eigenvalue of the phonon corresponding to the branch index  $s$ ,  $\tau$  is the reciprocal lattice vector,  $d$  is the atom index in the unit cell,  $\mathbf{r}_d$  is the atom position,  $W_d$  is the corresponding Debye-Waller factor, and  $\mathbf{e}_{ds}$  is the phonon eigenvectors.

### B. Thermal transport calculation

The temperature-dependent phonon dispersion was calculated based on the temperature-dependent effective potential (TDEP) method [27–29]. The moment tensor potential (MTP) developed by Shapeev *et al.* [30], which is one of the machine learning interaction potentials, was applied to conduct molecular dynamics (MD) by LAMMPS to provide reliable forces and displacements in order to extract force constants by TDEP. The data used to train the MTP are obtained from *ab initio* molecular dynamics (AIMD) simulations performed using the Vienna *Ab initio* Simulation Package (VASP). [31] The local density approximation (LDA) was used in the AIMD simulation. The kinetic energy cutoff and electronic energy tolerance were set as 500 and  $10^{-5}$  eV, respectively. The  $K$  points were chosen as  $\Gamma$  only. The cubiclike supercell with 208 atoms was utilized to efficiently reduce the computational cost of acquiring phonon dispersions [32,33]. The experimental thermal expansion was applied to the calculation [34]. The AIMD simulations were run for 1500 steps with a time step of 1 fs/step at 300, 600, and 900 K. These simulations utilized the canonical ensemble with a Nosé-Hoover thermostat. Configurations for the training potential were selected every ten steps at the above-mentioned three temperatures (a total of 450 configurations). The MTP with a maximum level of 16 was applied. The minimum and maximum cutoff radius for the MTP was chosen to be 1.6 and 10 Å. The fitting weights of energies, forces, and stresses were set as 1, 0.1, and 0.01 in the training processes, respectively. According to the validation set, the root mean square error (RMSE) of energies and forces are 0.00068 meV/atom and 0.021 meV/Å, respectively. More validation data are shown in Fig. S2 [26], including the validation of energy and force.

The force constants at 0 K were calculated by the finite displacement method based on the density functional theory (DFT) using VASP and PHONOPY packages. The primitive cell was fully relaxed with the kinetic energy cutoff of 600 eV, the electronic energy tolerance of  $10^{-8}$  eV, and the force tolerance of  $10^{-6}$  eV/Å. The lattice constants after relaxed are  $a = b = 3.16$  Å,  $c = 5.15$  Å, which are slightly smaller than the experimental values  $a = b = 3.191$  Å,  $c = 5.191$  Å

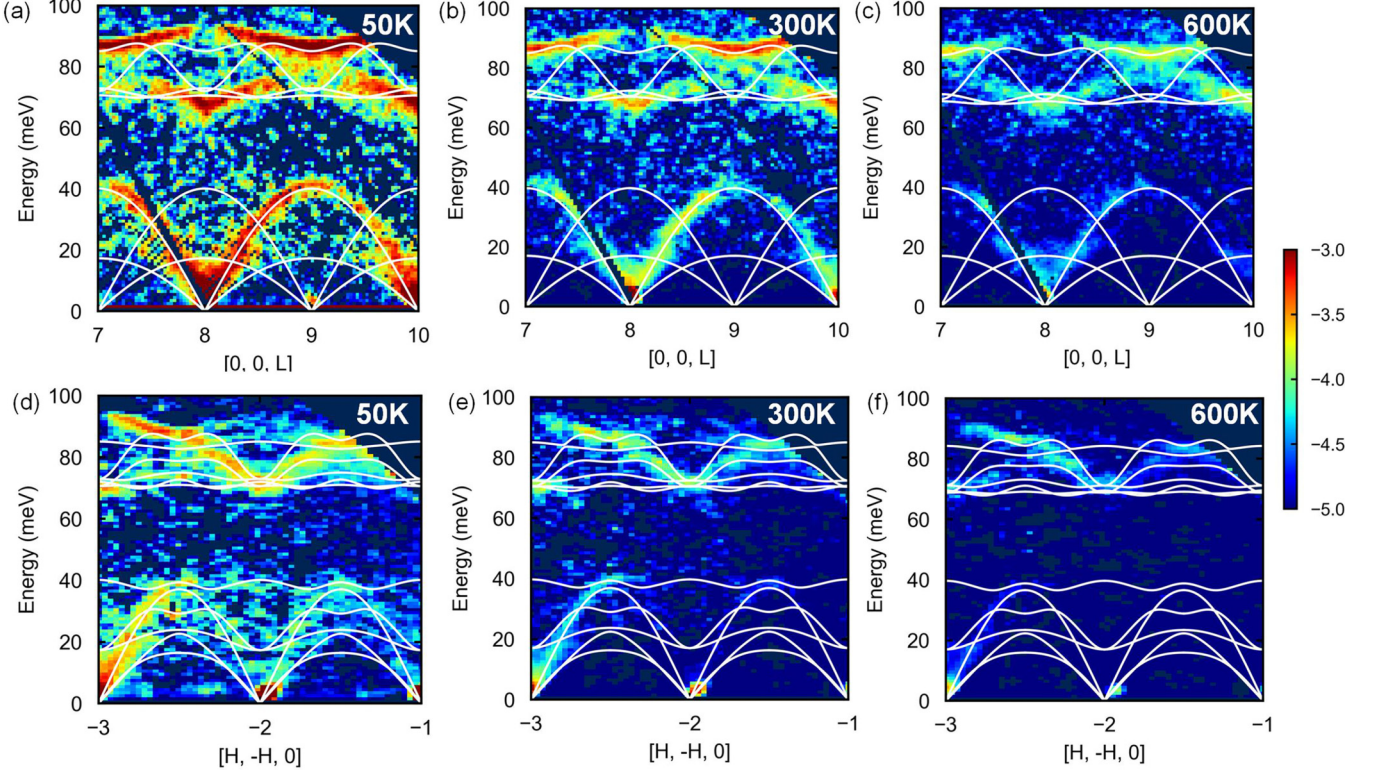


FIG. 1. Comparison between the measured  $\chi''(\mathbf{Q}, E)$  and the temperature-dependent calculated phonon dispersions. (a)–(c) are the results along  $[0, 0, L]$  direction at 50, 300, and 600 K, respectively. (c)–(e) are the results along  $[H, -H, 0]$  direction at 50, 300, and 600 K, respectively. The logarithmic color bar indicates the intensity. White lines are the calculated temperature-dependent phonon dispersions with MTP.

[19]. The  $K$  point was set as  $12 \times 12 \times 9$ . The harmonic force constants are acquired using the PHONOPY package [35] with a  $4 \times 4 \times 3$  supercell of GaN. The quasiharmonic approximation (QHA) calculation was conducted with the help of the PHONOPY package.

Then, the MD simulation with MTP by the LAMMPS package [36] was utilized to acquire the converged phonon dispersion. The  $10 \times 10 \times 5$  supercell was applied after the convergence test at 300 K, as shown in Fig. S3 [26]. The supercell was first relaxed 5 ps with the  $NVT$  ensemble and was changed to run with the  $NVE$  ensemble to collect displacements and forces for 2.44 ns at 50, 300, 600, and 900 K. The cutoff distance of second-order, third-order, and fourth-order force constants was set as 7, 7, and 3 Å, as shown in the converged test in Fig. S4 [26]. The temperature-dependent thermal conductivity was calculated with FOURPHONON [37], which includes the four-phonon scattering processes by solving the Boltzmann transport equation. The converged  $q$  mesh  $13 \times 13 \times 13$  was chosen to calculate thermal conductivity.

### III. RESULTS

Figure 1 shows the measured dynamical susceptibility,  $\chi''(\mathbf{Q}, E)$ , by INS of GaN with two-dimensional slices along both in-plane ( $[H, -H, 0]$ ) and out-of-plane ( $[0, 0, L]$ ) directions at 50, 300, and 600 K, respectively, superimposed on the calculations with the corresponding temperature. The temperature-dependent calculation of the low-energy ( $<40$  meV) phonon dispersion agrees well with the experimental result, although that of the high-energy ( $>60$  meV)

one has slightly more difference at each temperature. Such discrepancy also exists compared to other harmonic phonon calculations. It may be related to the little local density approximation potential inaccuracy [19,38,39], which reflects the difference between experimental and calculated lattice constants. The error may be transmitted to the training database. However, on the whole, the calculation based on the machine-learning potential can be regarded as a reproduction of the experimental results, indicating that our calculation is reliable.

Figure 2 illustrates the comparison between the measured and calculated temperature-dependent phonon DOS. The neutron-weighted phonon DOS  $g(E)$  was calculated by  $g_{NW}(E) = (\frac{\sigma_{Ga}}{m_{Ga}} g_{Ga}(E) + \frac{\sigma_N}{m_N} g_N(E)) / (\frac{\sigma_{Ga}}{m_{Ga}} + \frac{\sigma_N}{m_N})$ , where  $g_{Ga}(E)$  and  $g_N(E)$  are partial phonon DOS of Ga and N, respectively [40]. The  $\sigma_{Ga}$  ( $\sigma_N$ ) and  $m_{Ga}$  ( $m_N$ ) indicate the neutron cross section of Ga(N) and the relative atomic mass of Ga(N), respectively. It is found that there are four peaks in the phonon DOS, and each peak contains several branches. With increasing temperature, the low-energy peak 1 ( $P1$ ) broadens and gradually splits into a peak and a shoulder, while peaks 2, 3, and 4 ( $P2$ – $P4$ ) all exhibit an obvious softening. It is well known that phonons and their linewidths will soften and broaden respectively with increasing temperature when the system has strong anharmonic effects [41]. Thus, due to different degrees of anharmonicity of phonons, branches in a DOS peak will show different degrees of softening, resulting in the overall peak softening or broadening. With the presence of phonon linewidths in the INS data, the shape changes of these four DOS peaks indicate moderate anharmonicity of GaN

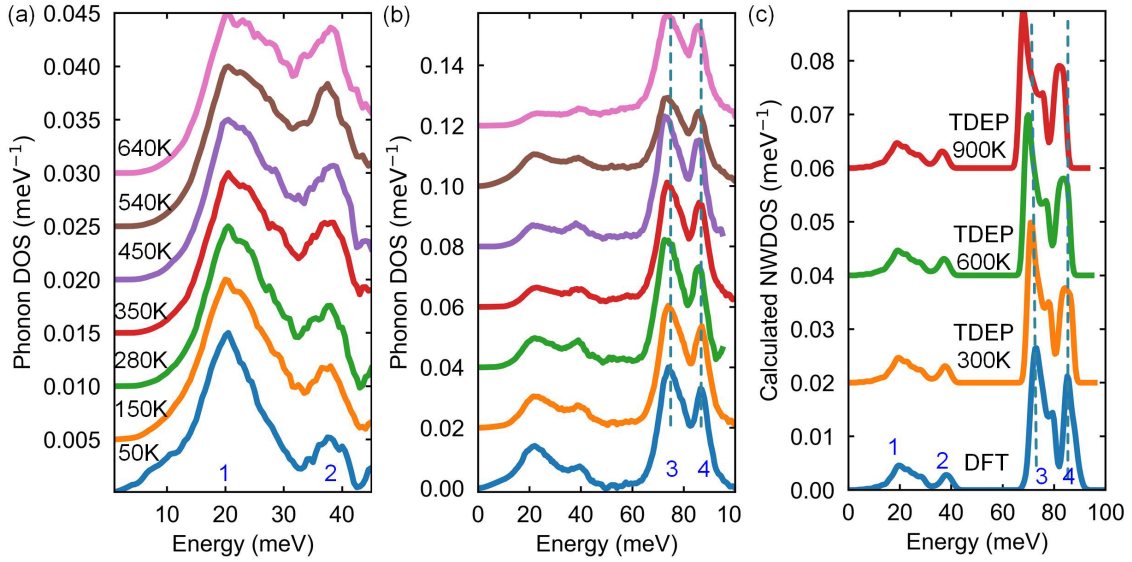


FIG. 2. The temperature-dependent phonon density of state (DOS). Measured phonon DOS with incident energy of 50 (a) and 150 meV (b) at different temperatures are normalized to unity. (c) Calculated neutron-weighted phonon DOS with 0 (dark blue), 300 (orange), 600 (green), and 900 K (red). Numbers in (a) and (b) indicate the different peaks in the phonon DOS. Dashed lines are the eye guidance to identify the phonon softening with increasing temperature.

[Figs. 2(a) and 2(b)]. The temperature-dependent calculation reproduces the similar temperature-dependent DOS behavior well. In Fig. 2(c), it can be seen that peaks 3 and 4 calculated by DFT and MD soften gradually with temperature rises from 0 to 900 K, indicating the significance of the anharmonicity.

To clearly show its temperature dependence, the Gaussian function is utilized to extract the centers of  $P2$ – $P4$ , as shown in Fig. 3(a). It should be noted that  $P1$  has little change with temperature due to relatively weak anharmonicity, which is also predicted by Herriman *et al.* [25].  $P3$  and  $P4$ , which correspond to the high energy optical phonon modes, soften faster than the low-energy  $P2$  at high temperature. The mode Grüneisen parameter,  $\gamma_i = -\frac{\partial \ln \varepsilon_i}{\partial \ln V}$ , is used here to evaluate the anharmonicity of these DOS peaks by taking the derivative of phonon mode energy ( $\varepsilon_i$ ) and crystal volume ( $V$ ) at finite temperature [42]. With the temperature-dependent  $V$  [34], the experimental  $\gamma_{P3-P4}$  with  $\gamma_{P3} = 2.96 \pm 1.23$  and  $\gamma_{P4} = 3.09 \pm 0.97$  were acquired, similar to the calculated

$\gamma_{P3\_cal} = 3.56 \pm 0.20$  and  $\gamma_{P4\_cal} = 3.80 \pm 0.03$ . This result confirms the high sensitivity of the high-energy optical modes to temperature, indicating strong anharmonicity of  $P3$  and  $P4$ , which is in good agreement with the prediction of Herriman *et al.* [43].

Although the anharmonicity of the phonon DOS peaks is well evaluated by the calculated and experimental Grüneisen parameters, the high (third and fourth)-order contributions are difficult to be distinguished. The vibrational entropy based on the phonon DOS was introduced to further explore the anharmonic effect, defined as [42,44]

$$S_{\text{vib}} = 3k_B \int d\varepsilon g(\varepsilon) \{ [n(\varepsilon) + 1] \ln [n(\varepsilon) + 1] - n(\varepsilon) \times \ln [n(\varepsilon)] \}, \quad (2)$$

where  $g(\varepsilon)$  is the phonon DOS normalized to 1,  $n(\varepsilon)$  is the Plack distribution, and  $k_B$  is the Boltzmann constant. As

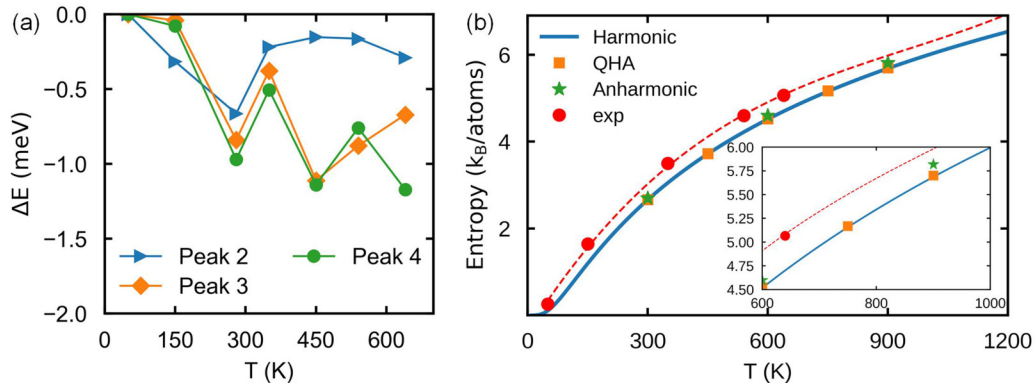


FIG. 3. (a) Temperature-dependent fitting results of Gaussian function for three DOS peaks in Fig. 2. (b) Temperature-dependent vibrational entropy of GaN from experimental phonon DOS (circles), harmonic (blue lines), QHA (orange squares), and anharmonic calculation (stars). Dashed spline curve shows the trend of the experimental results at high temperatures.

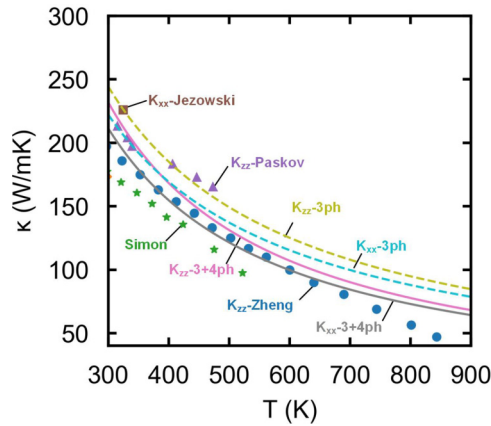


FIG. 4. Temperature-dependent thermal conductivity of GaN. The dashed and solid lines indicate the fitting of calculations, including three-phonon scattering processes and both three- and four-phonon scattering processes, respectively. The dots are experimental results [14,48–51].

shown in Fig. 3(b), the calculated vibrational entropy with the harmonic approximation has a growing difference with the experimental results as the temperature increases. It should be noted that over the whole temperature range, the experimental result is slightly larger than the calculation, which may result from the imperfect exchange-potential function in the calculation. Besides, the imperfection of GaN is unavoidable, which may include some dislocation-induced strain or impurity to affect the vibrational entropy [45,46]. At 50 K, the difference between calculation with harmonic approximation and experiment is  $\sim 0.13 k_B/\text{atom}$ . When the temperature increases to 640 K, the difference between the calculation with harmonic approximation and the experiment increases to  $\sim 0.37 k_B/\text{atom}$ . The difference between quasiharmonic approximation (QHA) and the experiment is  $\sim 0.36 k_B/\text{atom}$  at 640 K, which indicates the QHA is insufficient to describe the temperature-dependent entropy. However, when including the anharmonicity, the difference between the calculation and experiment decreases to  $\sim 0.28 k_B/\text{atom}$ , representing a decrease of  $\sim 22\%$  compared to the difference between the calculation with harmonic approximation and the experiment. The temperature-dependent calculation can effectively decrease the difference between the calculation with harmonic approximation and the experiment, further underlining the significance of the anharmonic effect at high temperatures in GaN [inset picture in Fig. 3(b)].

Therefore, the INS measurement indicates the non-negligible anharmonicity in GaN at high temperatures. Such change of phonon modes with temperature will lead to the evolution of lattice thermal conductivity, closely related to the high-order phonon scattering processes. As shown in Fig. 4, the calculated thermal conductivity with three- and four-phonon (3+4ph) scattering processes agrees better with previous measurements than that only with three-phonon (3ph) scattering processes at high temperatures. The inclusion of four-phonon scattering processes further decreases the thermal conductivity closer to the experimental result, especially at high temperatures. Besides, the temperature-dependent thermal conductivity along the  $zz$  direction changes

from  $\kappa \sim T^{-1}$  to  $\kappa \sim T^{-1.12}$  after including the four-phonon scattering processes, much closer to the  $\sim T^{-1.2}$  reported by Slack *et al.* [47] and Jezowski *et al.* [48]. Notably, the thermal conductivity still shows a difference between our 3+4ph results and the experiment at around 800 K. The emergence of such difference may be due to the limitation of TDTR experiment, where the GaN sample with dislocations was used for the thermal conductivity measurement in Ref. [14]. For example, with a relatively large laser spot size, the TDTR measurement is insensitive to heat transfer in the in-plane direction [14]. Nevertheless, our calculation, including the four-phonon interaction, at least appears to be more consistent with experimental values. Thus, the four-phonon scattering plays a vital role in correcting the thermal conductivity of GaN at high temperatures, which further indicates the failure of the description of anharmonicity by low-order phonon interaction at high temperatures.

The temperature-dependent calculation of thermal conductivity in Fig. 4 also indicates that the anisotropy of thermal conductivity in GaN decreases obviously with the temperature increases. The ratio of the thermal conductivity along the  $zz$  and  $xx$  directions,  $\kappa_{zz}/\kappa_{xx}$ , decreases from 1.098 at 300 K to 1.059 at 900 K when only considering three-phonon scattering processes. However, when including the four-phonon scattering processes, the ratio of  $\kappa_{zz}/\kappa_{xx}$  decreases from 1.097 at 300 K to 1.048 at 900 K, which indicates that the four-phonon scattering process contributes to the reduced anisotropy. The ratio of lattice constants  $c/a$  decreases from 1.628 to 1.627 as the temperature increases from approximately 300 K to around 900 K. This suggests that a decreased thermal conductivity anisotropy in GaN at elevated temperatures is reasonable [32]. Notably, the lower  $\kappa_{xx}$  is well revealed by the in-plane Matryoshka phonon twinning behavior at 300 K, which enriches the three-phonon scattering channels [19].

Figure 5 further illustrates the effect of four-phonon scattering processes on thermal conductivity along the  $xx$  and  $zz$  directions at 900 K in detail. The cumulative thermal conductivity in Figs. 5(a) and 5(c) indicates that the phonon modes below 30 meV contribute to the most thermal conductivity, mainly from the acoustic phonon modes. The energy-dependent thermal conductivity in Figs. 5(b) and 5(d) illustrate that the phonon modes between 20 and 30 meV have the non-negligible contribution of four-phonon interaction. This energy region corresponds to the significantly wider area of  $P1$  in DOS, as shown in Fig. 2(a). Only considering three-phonon scattering processes leads to the overestimation of thermal conductivity of GaN as  $\kappa_{xx} = 75.89$  W/mK and  $\kappa_{zz} = 80.41$  W/mK at 900 K. The inclusion of the four-phonon scattering process well corrects the thermal conductivity of GaN as  $\kappa_{xx} = 62.26$  W/mK and  $\kappa_{zz} = 65.27$  W/mK at 900 K.

To further understand the contribution of four-phonon scattering processes between 20 and 30 meV, the phonon from three- and four-phonon scattering processes are shown in Fig. 6(a). It is found that the linewidths from four-phonon scattering processes become comparable with those from three-phonon scattering processes between 20 and 30 meV, which is mainly attributed to the big four-phonon scattering phase space in this energy region [Fig. 6(b)]. Thus, the

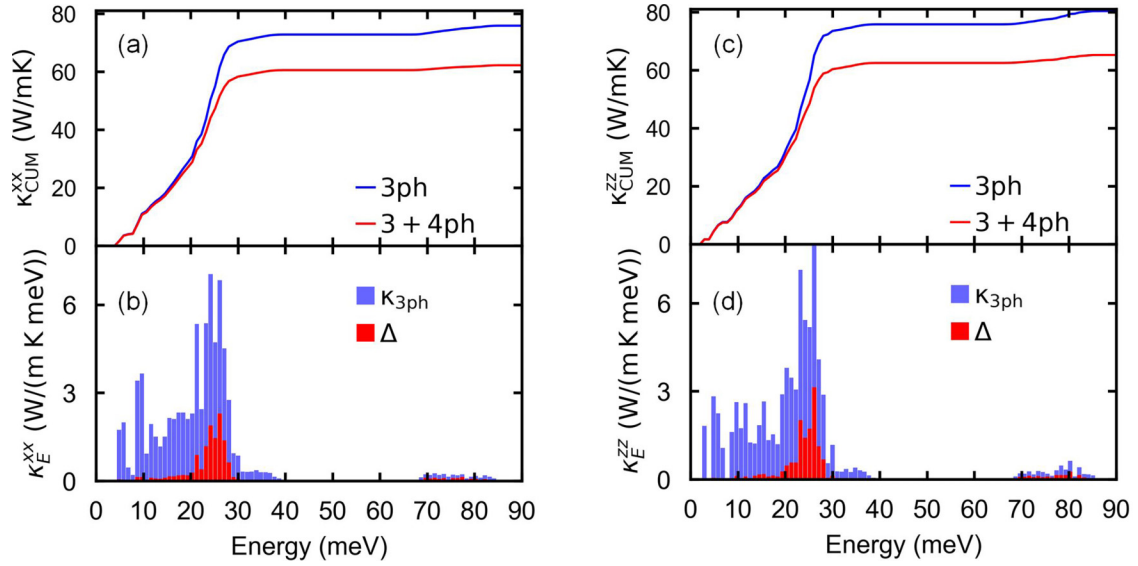


FIG. 5. Cumulative thermal conductivity along  $xx$  (a) and  $zz$  (c) direction at 900 K. Blue and red lines indicate the results including only three-phonon and both three- and four-phonon scattering processes, respectively. Energy-dependent thermal conductivity of GaN along  $xx$  (b) and  $zz$  (d) direction at 900 K. Blue bars indicate the energy-dependent thermal conductivity from three-phonon interaction  $\kappa_{3\text{ph}}$  while red bars indicate the effect of four-phonon scattering processes, which is described as  $\Delta = |\kappa_{3+4\text{ph}} - \kappa_{3\text{ph}}|$ .

three-phonon scattering processes are strongly suppressed here, but the four-phonon scattering processes are enhanced. As shown in Fig. S5 [26], the acoustic ( $A$ ) phonon bands become bunched together when the  $q$  vector approaches the zone boundary in GaN [16,52]. Besides, there is a phonon band gap  $\Delta\omega_{A-O} \sim 25$  meV, related to the relatively large Ga-to-N mass ratio  $\sim 5$ . This gap will also lead to the dip of  $AAO$  processes around 20 meV. The  $AAO$  ( $O$  is optical phonon mode) process will be prohibited if one of the participating acoustic phonons has a frequency below the frequency gap. Such behavior leads to the small phase space for  $AAO$  around 20 meV [Fig. 6(c)]. For the  $AAO$  process, as the acoustic phonon modes approach the optical phonon bandwidth, the available  $AAO$  scattering channels decrease. This decrease occurs because the  $AAO$  process cannot take place when they

involve acoustic phonons with frequencies exceeding the optic phonon bandwidth, which is the main reason that there is a dip of  $AAO$  between 20 and 30 meV, as marked in Fig. 6(c). Therefore, these critical three-phonon selection rules lead to the small scattering phase space between 20 and 30 meV. However, the acoustic bunching and phonon band gap have little influence on the four-phonon scattering processes [52]. As a result, four-phonon scattering processes become more important at high temperatures due to anharmonicity, which greatly affects thermal conductivity.

#### IV. CONCLUSION

In summary, we explore the high-order phonon anharmonicity and thermal conductivity of GaN, especially at

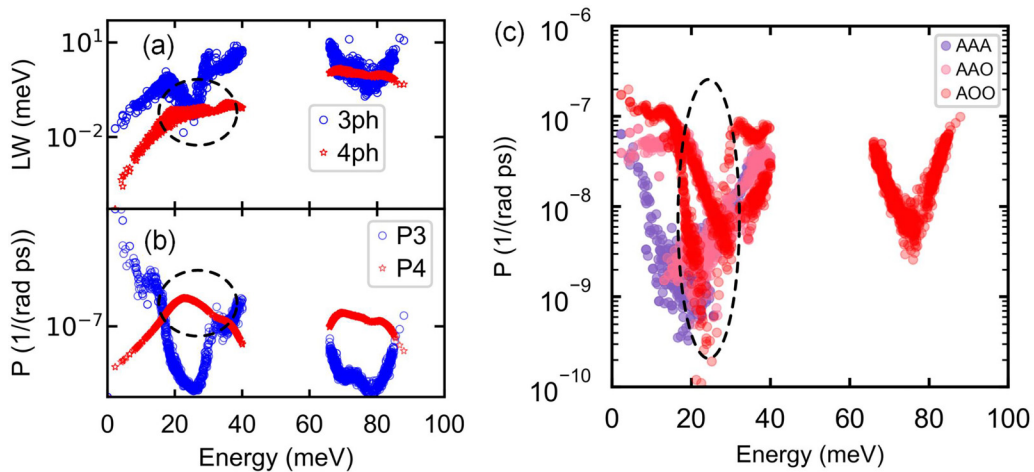


FIG. 6. (a) Energy-dependent phonon linewidth of GaN. (b) Energy-dependent phonon scattering phase space. The circles and stars in (a) and (b) indicate the contribution from three-phonon and four-phonon scattering processes, respectively. (c) Detailed three-phonon scattering processes. The  $A$  and  $O$  indicate the acoustic and optical phonon modes, respectively.

high temperatures. The inelastic neutron scattering experiment and MLIP-based calculation confirm the softened phonon modes at high temperatures. The high-energy optical phonon modes possess large Grüneisen parameters. The vibrational entropy calculation, which considers temperature-induced anharmonicity, matches the experimental results better than the calculation based on harmonic approximation at high temperatures. The larger anharmonicity at high temperatures also leads to the more obvious four-phonon scattering processes. The inclusion of four-phonon scattering processes aligns well with the calculated and experimentally observed thermal conductivity. Along with the critical selection rule limited three-phonon scattering, the four-phonon scattering processes, especially between 20 and 30 meV, play more essential roles in the total lattice thermal conductivity at high temperature. Our work deepens the understanding of phonon property and its temperature dependence in GaN and highlights the role of the high-order

phonon process in studying the thermal conductivity at high temperatures.

## ACKNOWLEDGMENTS

This work was financially supported by the Basic Science Center Project of the National Natural Science Foundation of China under Grant No. 52388201. The work by Y.L. and J.H. was supported by supported by the National Key R&D Program of China (Grant No. 2021YFA1400300) and the Beijing Natural Science Foundation (Grant No. Z190011). The work by Q.S. and C.L. was supported by the National Science Foundation under Grant No. 2227947. B.W. acknowledges the support by the National Science Foundation of China (Grant No. 12304040), China Postdoctoral Science Foundation (Grant No. 2023M742004), and the State Key Laboratory of New Ceramic and Fine Processing Tsinghua University (Grant No. KF202304).

- 
- [1] H. Amano, Y. Baines, E. Beam, M. Borga, T. Bouchet, P. R. Chalker, M. Charles, K. J. Chen, N. Chowdhury, R. Chu *et al.*, The 2018 GaN power electronics roadmap, *J. Phys. D: Appl. Phys.* **51**, 163001 (2018).
- [2] L. Lindsay, D. A. Broido, and T. L. Reinecke, Thermal conductivity and large isotope effect in GaN from first principles, *Phys. Rev. Lett.* **109**, 095901 (2012).
- [3] K. Chung, C.-H. Lee, and G.-C. Yi, Transferable GaN layers grown on ZnO-Coated graphene layers for optoelectronic devices, *Science* **330**, 655 (2010).
- [4] K. Ebrahimi, G. F. Jones, and A. S. Fleischer, A review of data center cooling technology, operating conditions and the corresponding low-grade waste heat recovery opportunities, *Renew. Sust. Energ. Rev.* **31**, 622 (2014).
- [5] D.-S. Tang and B.-Y. Cao, Phonon thermal transport and its tunability in GaN for near-junction thermal management of electronics: A review, *Int. J. Heat Mass Transfer* **200**, 123497 (2023).
- [6] A. K. Morya, M. C. Gardner, B. Anvari, L. Liu, A. G. Yepes, J. Doval-Gandoy, and H. A. Toliyat, Wide bandgap devices in AC electric drives: Opportunities and challenges, *IEEE Trans. Transp. Electrification* **5**, 3 (2019).
- [7] M. Yang, M.-T. Li, Y.-C. Hua, W. Wang, and B.-Y. Cao, Experimental study on single-phase hybrid Microchannel cooling using HFE-7100 for liquid-cooled chips, *Int. J. Heat Mass Transfer* **160**, 120230 (2020).
- [8] X.-Y. Liu, H.-Q. Zhang, B.-B. Li, J. Liu, D.-Y. Xue, H.-S. Wang, H.-W. Liang, and X.-C. Xia, Characteristics of AlGaIn/GaN high electron mobility transistor temperature sensor, *Acta Phys. Sin.* **69**, 047201 (2020).
- [9] O. Semenov, A. Vassighi, and M. Sachdev, Impact of self-heating effect on long-term reliability and performance degradation in CMOS circuits, *IEEE Trans. Dev. Mater. Reliab.* **6**, 17 (2006).
- [10] Y. Zhao and Y. Qu, Impact of self-heating effect on transistor characterization and reliability issues in Sub-10 Nm technology nodes, *IEEE J. Electron Dev. Soc.* **7**, 829 (2019).
- [11] R. Wang, J. Zhuge, R. Huang, D.-W. Kim, D. Park, and Y. Wang, Investigation on self-heating effect in gate-all-around silicon nanowire MOSFETs from top-down approach, *IEEE Electron Dev. Lett.* **30**, 559 (2009).
- [12] A. Bar-Cohen, J. J. Maurer, and A. Sivanathan, Near-Junction microfluidic thermal management of RF power amplifiers, in *2015 IEEE International Conference on Microwaves, Communications, Antennas and Electronic Systems (COMCAS) Tel Aviv, Israel* (IEEE, Piscataway, NJ, 2015), pp. 1–8.
- [13] Y.-C. Hua, H.-L. Li, and B.-Y. Cao, Thermal spreading resistance in ballistic-diffusive regime for GaN HEMTs, *IEEE Trans. Electron Dev.* **66**, 3296 (2019).
- [14] Q. Zheng, C. Li, A. Rai, J. H. Leach, D. A. Broido, and D. G. Cahill, Thermal conductivity of GaN, <sup>71</sup>GaN, and SiC from 150 K to 850 K, *Phys. Rev. Mater.* **3**, 014601 (2019).
- [15] B. Sun, G. Haunschild, C. Polanco, J. (Zi.-J.) Ju, L. Lindsay, G. Koblmüller, and Y. K. Koh, Dislocation-induced thermal transport anisotropy in single-crystal group-III nitride films, *Nat. Mater.* **18**, 136 (2019).
- [16] X. Yang, T. Feng, J. Li, and X. Ruan, Stronger role of four-phonon scattering than three-phonon scattering in thermal conductivity of III-V semiconductors at room temperature, *Phys. Rev. B* **100**, 245203 (2019).
- [17] S. Li, S. Liu, Y. Tian, C. Zhang, J. Wei, X. Tao, N. Li, L. Zhang, and W. Sun, High-Temperature electrical performances and physics-based analysis of p-GaN HEMT device, *IET Power Electron.* **13**, 420 (2020).
- [18] P. Herfurth, D. Maier, Y. Men, R. Rösch, L. Lugani, J.-F. Carlin, N. Grandjean, and E. Kohn, GaN-on-Insulator technology for high-temperature electronics beyond 400 °C, *Semicond. Sci. Technol.* **28**, 074026 (2013).
- [19] B. Wei, Q. Cai, Q. Sun, Y. Su, A. H. Said, D. L. Abernathy, J. Hong, and C. Li, Matryoshka phonon twinning in  $\alpha$ -GaN, *Commun. Phys.* **4**, 227 (2021).
- [20] T. Ruf, J. Serrano, M. Cardona, P. Pavone, M. Pabst, M. Krisch, M. D’Astuto, T. Suski, I. Grzegory, and M. Leszczynski, Phonon dispersion curves in wurtzite-structure GaN determined by inelastic x-ray scattering, *Phys. Rev. Lett.* **86**, 906 (2001).

- [21] F. Tian, B. Song, X. Chen, N. K. Ravichandran, Y. Lv, K. Chen, S. Sullivan, J. Kim, Y. Zhou, T.-H. Liu *et al.*, Unusual high thermal conductivity in boron arsenide bulk crystals, *Science* **361**, 582 (2018).
- [22] J. S. Kang, M. Li, H. Wu, H. Nguyen, and Y. Hu, Experimental observation of high thermal conductivity in boron arsenide, *Science* **361**, 575 (2018).
- [23] L. Xie, J. H. Feng, R. Li, and J. Q. He, First-Principles study of anharmonic lattice dynamics in low thermal conductivity  $\text{AgCrSe}_2$ : Evidence for a large resonant four-phonon scattering, *Phys. Rev. Lett.* **125**, 245901 (2020).
- [24] X. Song, Y. Zhao, J. Ni, S. Meng, and Z. Dai, Strong anharmonic phonon scattering and superior thermoelectric properties of  $\text{Li}_2\text{NaBi}$ , *Mater. Today Phys.* **31**, 100990 (2023).
- [25] T. Yue, Y. Zhao, J. Ni, S. Meng, and Z. Dai, Strong quartic anharmonicity, ultralow thermal conductivity, high band degeneracy and good thermoelectric performance in  $\text{Na}_2\text{TlSb}$ , *npj Comput. Mater.* **9**, 17 (2023).
- [26] See Supplemental Material at <http://link.aps.org/supplemental/10.1103/PhysRevB.109.155204> for the reciprocal space map of elastic scattering ( $-1.5 \leq E \leq 1.5$  meV) measurements at ARCS; the comparisons of energy and force between MTP and DFT calculations; the converged supercell size for calculation of phonon dispersion at 300 K; the cutoff distance dependent coefficient of determination in order to extract the second-order, third-order, and fourth-order force constants; the calculated phonon dispersion at 300 and 900 K.
- [27] O. Hellman, I. A. Abrikosov, and S. I. Simak, Lattice dynamics of anharmonic solids from first principles, *Phys. Rev. B* **84**, 180301(R) (2011).
- [28] O. Hellman, P. Steneteg, I. A. Abrikosov, and S. I. Simak, Temperature dependent effective potential method for accurate free energy calculations of solids, *Phys. Rev. B* **87**, 104111 (2013).
- [29] O. Hellman and I. A. Abrikosov, Temperature-Dependent effective third-order interatomic force constants from first principles, *Phys. Rev. B* **88**, 144301 (2013).
- [30] I. S. Novikov, K. Gubaev, E. V. Podryabinkin, and A. V. Shapeev, The MLIP Package: Moment tensor potentials with MPI and active learning, *Mach. Learn.* **2**, 025002 (2021).
- [31] G. Sun, J. Kürti, P. Rajczy, M. Kertesz, J. Hafner, and G. Kresse, Performance of the vienna ab initio simulation package (VASP) in chemical applications, *J. Mol. Struct.* **624**, 37 (2003).
- [32] Y. Li, J. Liu, and J. Hong, Anharmonicity-Induced strong temperature-dependent thermal conductivity in  $\text{CuInX}_2$  ( $X = \text{Se}, \text{Te}$ ), *Phys. Rev. B* **106**, 094317 (2022).
- [33] J. H. Lloyd-Williams and B. Monserrat, Lattice dynamics and electron-phonon coupling calculations using nondiagonal supercells, *Phys. Rev. B* **92**, 184301 (2015).
- [34] H. Iwanaga, A. Kunishige, and S. Takeuchi, Anisotropic thermal expansion in wurtzite-type crystals, *J. Mater. Sci.* **35**, 2451 (2000).
- [35] A. Togo, L. Chaput, T. Tadano, and I. Tanaka, Implementation strategies in phonopy and phono3py, *J. Phys.: Condens. Matter* **35**, 353001 (2023).
- [36] A. P. Thompson, H. M. Aktulga, R. Berger, D. S. Bolintineanu, W. M. Brown, P. S. Crozier, P. J. In't Veld, A. Kohlmeyer, S. G. Moore, T. D. Nguyen *et al.*, LAMMPS - a flexible simulation tool for particle-based materials modeling at the atomic, Meso, and continuum scales, *Comput. Phys. Commun.* **271**, 108171 (2022).
- [37] Z. Han, X. Yang, W. Li, T. Feng, and X. Ruan, Four-Phonon: An extension module to ShengBTE for computing four-phonon scattering rates and thermal conductivity, *Comput. Phys. Commun.* **270**, 108179 (2022).
- [38] J.-Y. Yang, G. Qin, and M. Hu, Nontrivial contribution of fröhlich electron-phonon interaction to lattice thermal conductivity of wurtzite GaN, *Appl. Phys. Lett.* **109**, 242103 (2016).
- [39] D. Q. Tran, T. Paskova, V. Darakchieva, and P. P. Paskov, On the thermal conductivity anisotropy in wurtzite GaN, *AIP Adv.* **13**, 095009 (2023).
- [40] M. S. Lucas, J. A. Muñoz, O. Delaire, N. D. Markovskiy, M. B. Stone, D. L. Abernathy, I. Halevy, L. Mauger *et al.*, Effects of composition, temperature, and magnetism on phonons in Bcc Fe-V alloys, *Phys. Rev. B* **82**, 144306 (2010).
- [41] B. Wei, Q. Sun, C. Li, and J. Hong, Phonon anharmonicity: A pertinent review of recent progress and perspective, *Sci. China Phys. Mech. Astron.* **64**, 117001 (2021).
- [42] D. S. Kim, H. L. Smith, J. L. Niedziela, C. W. Li, D. L. Abernathy, and B. Fultz, Phonon anharmonicity in silicon from 100 to 1500 K, *Phys. Rev. B* **91**, 014307 (2015).
- [43] J. E. Herriman, O. Hellman, and B. Fultz, Phonon thermodynamics and elastic behavior of GaN at high temperatures and pressures, *Phys. Rev. B* **98**, 214105 (2018).
- [44] B. Fultz, Vibrational thermodynamics of materials, *Prog. Mater. Sci.* **55**, 247 (2010).
- [45] M. Forsblom, N. Sandberg, and G. Grimvall, Vibrational entropy of dislocations in Al, *Philos. Mag.* **84**, 521 (2004).
- [46] M. E. Manley, W. L. Hults, J. C. Cooley, R. E. Hackenberg, D. J. Thoma, M. W. Koby, J. L. Smith, and K. Littrell, Vibration-Dominated negative mixing entropy for C impurities in  $\alpha$ -U, *Phys. Rev. B* **72**, 184302 (2005).
- [47] G. A. Slack, L. J. Schowalter, D. Morelli, and J. A. Freitas, Some effects of oxygen impurities on AlN and GaN, *J. Cryst. Growth* **246**, 287 (2002).
- [48] A. Jeżowski, B. A. Danilchenko, M. Boćkowski, I. Grzegory, S. Krukowski, T. Suski, and T. Paszkiewicz, Thermal conductivity of GaN crystals in 4.2–300 K range, *Solid State Commun.* **128**, 69 (2003).
- [49] A. Jeżowski, O. Churiukova, J. Mucha, T. Suski, I. A. Obukhov, and B. A. Danilchenko, Thermal conductivity of heavily doped bulk crystals GaN:O. Free carriers contribution, *Mater. Res. Express* **2**, 085902 (2015).
- [50] R. B. Simon, J. Anaya, and M. Kuball, Thermal conductivity of bulk GaN—Effects of oxygen, magnesium doping, and strain field compensation, *Appl. Phys. Lett.* **105**, 202105 (2014).
- [51] P. P. Paskov, M. Slomski, J. H. Leach, J. F. Muth, and T. Paskova, Effect of Si doping on the thermal conductivity of bulk GaN at elevated temperatures—theory and experiment, *AIP Adv.* **7**, 095302 (2017).
- [52] N. K. Ravichandran and D. Broido, Phonon-Phonon interactions in strongly bonded solids: Selection rules and higher-order processes, *Phys. Rev. X* **10**, 021063 (2020).